

On analytical construction of observable functions in extended dynamic mode decomposition for nonlinear estimation and prediction

Marcos Netto, *Member, IEEE*, Yoshihiko Susuki, *Member, IEEE*, Venkat Krishnan, *Senior Member, IEEE*, and Yingchen Zhang, *Senior Member, IEEE*

Abstract—We propose an analytical construction of observable functions in the extended dynamic mode decomposition (EDMD) algorithm. EDMD is a numerical method for approximating the spectral properties of the Koopman operator. The choice of observable functions is fundamental for the application of EDMD to nonlinear problems arising in systems and control. Existing methods either start from a set of dictionary functions and look for the subset that best fits, in a certain sense, the underlying nonlinear dynamics; or they rely on machine learning algorithms, e.g., neural networks, to “learn” observable functions that are not explicitly available. Conversely, we start from the dynamical system model and lift it through the Lie derivatives, rendering it into a polynomial form. This transformation into a polynomial form is exact, although not unique, and it provides an adequate set of observable functions. The strength of the proposed approach is its applicability to a broader class of nonlinear dynamical systems, particularly those with nonpolynomial functions and compositions thereof. Moreover, it retains the physical interpretability of the underlying dynamical system and can be readily integrated into existing numerical libraries. The proposed approach is illustrated with an application to electric power systems. The modeled system consists of a single generator connected to an infinite bus, in which case nonlinear terms include sine and cosine functions. The results demonstrate the effectiveness of the proposed procedure in off-attractor nonlinear dynamics for estimation and prediction; the observable functions obtained from the proposed construction outperformed existing methods that use dictionary functions comprising monomials or radial basis functions.

Index Terms—Extended dynamic mode decomposition, Koopman spectral analysis, Lie derivative, nonlinear estimation and prediction, observable function, polynomialization.

I. INTRODUCTION

KOOPMAN operator theory (KOT) and associated numerical methods [1]–[3] are promising for system identification [4], state estimation [5], stability assessment [6], and control [7] of nonlinear dynamical systems. The increasing interest in the applications of KOT to systems and control is primarily due to two of its characteristics: i) it does not rely on any model—from beginning to end, numerical methods based on KOT are truly data driven, yet they are supported

by a mathematical foundation anchored on the spectral theory of dynamical systems [1], [2]; and ii) linear and *nonlinear* modes are captured, although the numerical methods rely exclusively on linear algebra. In simple words, these outstanding characteristics can be explained by the fact that the Koopman operator is a linear, infinite-dimensional operator that acts on functions; in principle, any measured quantity of a dynamical system can be expressed as a function of its state variables, x , hereafter referred to as an observable function, $g(x)$. See, e.g., [1], [2] for a formal exposition of this topic.

A great deal of progress has been made in devising numerical methods that provide a finite-dimensional approximation to the infinite-dimensional Koopman operator. Extended dynamic mode decomposition (EDMD) [8] is an example of a powerful numerical method tailored to this purpose; see [9] for a study on the convergence of EDMD to the Koopman operator. EDMD is sensitive to the set of observable functions provided as input, however [10]; finding the right set of observable functions, i.e., a set of observable functions that yields a Koopman invariant subspace, is nontrivial [11] and an unsolved problem. Although there is an increase in the number of applications based on EDMD, very few researchers have tackled the fundamental challenge of choosing the right set of observable functions. One strategy is to start from a large set of dictionary functions and apply a sparse regression penalty on the number of functions selected to approximate the dynamics of the underlying system [12]. Another strategy is to use neural networks to “learn” the observable functions [10], [13], [14]. These strategies have found success in a broad range of complex problems where data are abundant and state-space models are scarce or nonexistent. A question that always plagues these strategies is how well the discovered mapping describes the underlying system dynamics *beyond* sampled trajectories. This is a challenging question to answer with limited to no access to a model.

On the other hand, state-space models are often available in systems and control. Although in certain cases the uncertainty in the parameters is large, the structure of the model is known. In this context, for a given set of observable functions, one can optimize the approximated spectral properties of the Koopman operator, in particular the Koopman eigenfunctions [15]. But the selection of observable functions is particularly challenging if the state-space model contains nonlinear terms given by non-polynomial functions and the underlying dynamical system has multiple fixed points [11]. Note that the Carleman linearization [16] is limited to polynomial vector fields. This problem has not been addressed before, and it is the main contribution of this letter.

Our investigations reveal that a broad class of dynamical systems comprise elementary nonlinear functions, such as $\sin x$, $\cos x$, e^x , $\frac{x}{k+x}$, and compositions of these elementary

This work was authored in part by the National Renewable Energy Laboratory (NREL), operated by Alliance for Sustainable Energy, LLC, for the U.S. Department of Energy (DOE) under contract no. DE-AC36-08GO28308. The views expressed in the article do not necessarily represent the views of the DOE or the U.S. Government. The U.S. Government and the publisher, by accepting the article for publication, acknowledges that the U.S. Government retains a nonexclusive, paid-up, irrevocable, worldwide license to publish or reproduce the published form of this work, or allow others to do so, for U.S. Government purposes.

M. Netto, V. Krishnan, and Y. Zhang are with the Power Systems Engineering Center, NREL, Golden, CO 80401, USA. Y. Susuki is with the Department of Electrical and Information Systems, Osaka Prefecture University, Osaka 599-8531, and JST, PRESTO, 4-1-8 Honcho, Kawaguchi, Saitama 332-0012, Japan.

Corresponding author: Marcos Netto (marcos.netto@nrel.gov).

functions; and that dynamical systems that fall into this class can be put into a polynomial form by lifting the original system to a space of higher dimension. The lifting procedure, originally proposed in [17], relies on Lie derivatives. We show that this embedding, referred to as *polynomialization*, makes EDMD more effective for the aforementioned class of dynamical systems. This letter is intended to set the direction for others working on the problem of selecting observable functions. Additionally, we envision the numerical illustration in Section IV to serve as a benchmark problem and solution that researchers could use to compare their choice of observable functions against.

II. PRELIMINARIES

A. Koopman Operator Theory

Let an autonomous dynamical system evolving on a finite, n -dimensional manifold \mathbb{X} be:

$$\dot{\mathbf{x}}(t) = \mathbf{f}(\mathbf{x}(t)), \quad (1)$$

for continuous time $t \in \mathbb{R}$, where $\mathbf{x} \in \mathbb{X}$ is the state, and $\mathbf{f} : \mathbb{X} \rightarrow T\mathbb{X}$ (tangent bundle of \mathbb{X}) is a nonlinear vector-valued function. In what follows, we introduce the Koopman operator for continuous time systems.

Let $g(\mathbf{x})$ be a scalar-valued function defined in \mathbb{X} , such that $g : \mathbb{X} \rightarrow \mathbb{C}$. The function g is referred to as *observable function*. The space of observable functions is $\mathcal{F} \subseteq C^0$, where C^0 denotes all continuous functions. Note that the choice of \mathcal{F} is discussed in [2].

The Koopman operator, denoted by \mathcal{K}_t , is a linear, infinite-dimensional operator [18] that acts on g in the following manner:

$$\mathcal{K}_t g := g \circ S_t, \quad (2)$$

where

$$S_t : \mathbb{X} \rightarrow \mathbb{X}; x(0) \rightarrow x(t) = x(0) + \int_0^t \mathbf{f}(\mathbf{x}(\tau)) d\tau \quad (3)$$

is called the *flow*.

The *Koopman eigenvalues*, λ , and *Koopman eigenfunctions*, $\phi(\mathbf{x})$, of the continuous time system (1) are such that:

$$\mathcal{K} \phi_i = e^{\lambda_i t} \phi_i, \quad i = 1, \dots, \infty, \quad (4)$$

where $\lambda_i \in \mathbb{C}$, and $\phi_i \in \mathcal{F}$ is nonzero. Now, consider a vector-valued function, $\mathbf{g} : \mathbb{X} \rightarrow \mathbb{C}^q$. If all elements of \mathbf{g} lie within the span of the Koopman eigenfunctions, then

$$\mathbf{g}(\mathbf{x}(t)) \approx \sum_{i=1}^{\infty} \phi_i(\mathbf{x}(t)) \mathbf{v}_i = \sum_{i=1}^{\infty} \phi_i(\mathbf{x}(0)) \mathbf{v}_i e^{\lambda_i t}, \quad (5)$$

where $\mathbf{v}_i \in \mathbb{C}^q$, $i = 1, \dots, q$, are referred to as *Koopman modes* [19].

B. Extended Dynamic Mode Decomposition

Consider pairs of snapshots of the system state variables, $\{\mathbf{x}_{k-1}, \mathbf{x}_k\}$, $k = 1, \dots, m$, as sampled data of continuous flows, i.e., under a sampling period Δt , we have $\mathbf{x}_k = \mathbf{x}(k\Delta t)$. The data matrices are defined as

$$\mathbf{X} = [\mathbf{x}_0 \dots \mathbf{x}_{m-1}], \quad \mathbf{X}^+ = [\mathbf{x}_1 \dots \mathbf{x}_m], \quad (6)$$

where $\mathbf{X}, \mathbf{X}^+ \in \mathbb{R}^{n \times m}$. The vector of observable functions is defined as

$$\mathbf{g}(\mathbf{x}_k) := [g_1(\mathbf{x}_k) \dots g_q(\mathbf{x}_k)]^\top, \quad (7)$$

where $\mathbf{g} : \mathbb{R}^n \rightarrow \mathbb{R}^q$, $q > n$. Also, the matrices of observables are defined as

$$\mathbf{G} = [\mathbf{g}(\mathbf{x}_0) \dots \mathbf{g}(\mathbf{x}_{m-1})], \quad \mathbf{G}^+ = [\mathbf{g}(\mathbf{x}_1) \dots \mathbf{g}(\mathbf{x}_m)], \quad (8)$$

where $\mathbf{G}, \mathbf{G}^+ \in \mathbb{R}^{q \times m}$. A finite-dimensional approximation to the Koopman operator is estimated as follows:

$$\mathbf{K} = \mathbf{G}^+ \mathbf{G}^\dagger, \quad (9)$$

where \mathbf{G}^\dagger denotes the Moore-Penrose pseudoinverse of \mathbf{G} , and $\mathbf{K} \in \mathbb{R}^{q \times q}$. The eigenvalues of \mathbf{K} are approximations to the Koopman eigenvalues, λ , whereas an approximation to the Koopman eigenfunctions is given by

$$\phi(\mathbf{x}_k) \approx \mathbf{L} \mathbf{g}(\mathbf{x}_k), \quad (10)$$

where the matrix \mathbf{L} contains the left eigenvectors of \mathbf{K} , and $\phi(\mathbf{x}_k) = [\phi_1(\mathbf{x}_k) \dots \phi_q(\mathbf{x}_k)]^\top$. Finally, to recover the Koopman modes for the full set of state variables $\mathbf{g}(\mathbf{x}_k) = \mathbf{x}_k$, let the projection matrix, $\mathbf{P} \in \mathbb{R}^{n \times q}$, be a matrix defined such that

$$\mathbf{x}_k = \mathbf{P} \mathbf{g}(\mathbf{x}_k). \quad (11)$$

From (10), we have that $\mathbf{g}(\mathbf{x}_k) = \mathbf{L}^{-1} \phi(\mathbf{x}_k)$, and thus

$$\mathbf{x}_k = \mathbf{P} \mathbf{g}(\mathbf{x}_k) = \mathbf{P} \mathbf{L}^{-1} \phi(\mathbf{x}_k). \quad (12)$$

Hence, an approximation to the Koopman modes is provided by the column vectors of $\mathbf{U} = \mathbf{P} \mathbf{L}^{-1}$, $\mathbf{U} \in \mathbb{C}^{n \times q}$, and

$$\mathbf{x}_k = \sum_{i=1}^q \phi_i(\mathbf{x}_k) \mathbf{v}_i = \sum_{i=1}^q \phi_i(\mathbf{x}_0) \mathbf{v}_i \lambda_i^k. \quad (13)$$

Note that (13) is a finite truncation of (5) under the sampling.

III. ANALYTICAL CONSTRUCTION OF OBSERVABLE FUNCTIONS

This section contains the main contribution of this letter. Let $\mathbb{X} \subseteq \mathbb{R}^n$ in the continuous time system (1). In what follows, we drop the time index, t , for simplicity. We are interested in the case where the nonlinear functions, $\mathbf{f}(\mathbf{x})$, can be written as a linear combination of elementary functions, $h(\mathbf{x}) \in \mathcal{F}$ —that is, if we consider the i -th state variable,

$$\dot{x}_i = \mathbf{k}_0^\top \mathbf{x} + k_1 h_1(\mathbf{x}) + \dots + k_m h_m(\mathbf{x}), \quad (14)$$

where \mathbf{k}_0^\top denotes the transpose of \mathbf{k}_0 .

The elementary functions include $\sin x$, $\cos x$, e^x , and $\frac{x}{k+x}$, as well as compositions of these elementary functions. Note that because of the composition of functions, these elementary functions encompass a broad class of models encountered in engineering, making this approach well-suited to applications of KOT. Indeed, mathematical models of many engineering systems can be written in the form of (14)—including models of ion channels [20], semiconductor devices [21], and power systems [22], [23]—thereby motivating the search for a state-inclusive Koopman observable space [24].

The following procedure was proposed in [17] as part of a model order reduction method, and it was recently applied in the context of system identification on a lifted space [25]. For each elementary function, $h_i(\mathbf{x})$, proceed as follows:

- 1) Introduce a new variable $z_i = h_i(\mathbf{x})$.
- 2) Replace $h_i(\mathbf{x})$ by z_i in the original equations.
- 3) Add $\dot{z}_i = \frac{\partial h_i(\mathbf{x})}{\partial \mathbf{x}} \mathbf{f}$ in the set of original equations.

The equation added in Step 3 is the Lie derivative of z_i with respect to \mathbf{f} . Note that Lie derivative is a Koopman generator in terms of the vector field \mathbf{f} . The resulting lifted system is as follows:

$$\dot{\mathbf{x}}_i = \mathbf{k}_0^\top \mathbf{x} + k_1 z_1 + \dots + k_m z_m, \quad (15)$$

$$\dot{z}_i = \mathcal{L}_{\mathbf{f}} h_i(\mathbf{x}), \quad (16)$$

where

$$\mathcal{L}_{\mathbf{f}} h_i(\mathbf{x}) = \frac{\partial h_i(\mathbf{x})}{\partial x_1} \dot{x}_1 + \dots + \frac{\partial h_i(\mathbf{x})}{\partial x_n} \dot{x}_n. \quad (17)$$

TABLE I
TRANSFORMATIONS FOR UNIVARIATE ELEMENTARY FUNCTIONS

Elementary function	New variable(s)	New differential equation(s)
$h(x) = e^x$	$z = e^x$	$\dot{z} = e^x = z$
$h(x) = \frac{1}{k+x}$	$z = \frac{1}{k+x}$	$\dot{z} = -\frac{1}{(k+x)^2} = -z^2$
$h(x) = x^k$	$z = x^k$	$\dot{z} = kx^{k-1} = kzx^{-1}$
$h(x) = \ln x$	$z = \ln x$	$\dot{z} = x^{-1}$
$h(x) = \sin x$	$z_1 = \sin x$ $z_2 = \cos x$	$\dot{z}_1 = \cos x = z_2$ $\dot{z}_2 = -\sin x = -z_1$

TABLE II
EXAMPLES OF POLYNOMIALIZATION OF SYSTEMS GIVEN BY
COMPOSITION OF ELEMENTARY FUNCTIONS

Original system	New variables	Lifted system
$\dot{x} = \frac{1}{1+e^x}$	$z_1 = e^x$ $z_2 = \frac{1}{1+z_1}$	$\dot{x} = z_2$ $\dot{z}_1 = e^x \frac{1}{1+e^x} = z_1 z_2$ $\dot{z}_2 = -\frac{1}{(1+z_1)^2} z_1 z_2 = -z_1 z_2^3$
$\dot{x} = x \cos x$	$z_1 = \cos x$ $z_2 = x z_1$ $z_3 = \sin x$ $z_4 = x z_3$	$\dot{x} = z_2$ $\dot{z}_1 = -\sin x (x \cos x) = -z_2 z_3 = -z_1 z_4$ $\dot{z}_2 = -x z_2 z_3 = -z_2 z_4$ $\dot{z}_3 = \cos x (x \cos x) = z_1 z_2$ $\dot{z}_4 = x z_1 z_2 = z_2^2$

Table I shows examples of transformations for univariate elementary functions, and the following remarks are in order:

- x^{-1} can be removed from the new differential equations by introducing another new variable, $y = x^{-1}$.
- There are elementary functions that need to be handled by adding two new variables, e.g., $\sin x$.

Now, for compositions of elementary functions, i.e., $h(x) = (h_1 \circ h_2)(x) = h_2(h_1(x))$, proceed as follows:

- 1) Introduce new variables $z_1 = h_1(x)$ and $z_2 = h_2(z_1)$.
- 2) Replace $h_2(h_1(x))$ by z_2 in the original equations.
- 3) Add $\dot{z}_1 = \frac{\partial h_1(x)}{\partial x} \mathbf{f}$ and $\dot{z}_2 = \frac{\partial h_2(z_1)}{\partial z_1} \dot{z}_1$ in the set of original equations.

Two examples of polynomialization involving the composition of elementary functions are given in Table II, from which two remarks are in order:

- Elementary functions that need to be handled by adding two new variables must be considered.
- Polynomialization is not a unique transformation, as is clear from the second example.

Note that polynomial systems obtained from the previous procedure can be put into a quadratic-linear form by applying another lifting. Moreover, the previous procedures also apply for control systems of the form:

$$\dot{x}_i = \mathbf{k}_0^T \mathbf{x} + k_1 h_1(x) + \dots + k_m h_m(x) + Bu, \quad (18)$$

where $u \in \mathbb{R}$ is the input. The interested reader is referred to [17]. Upon completion of the polynomialization, we select the state variables, along with the obtained new variables, as observable functions in the EDMD, i.e., $\{x_1, \dots, x_n, z_1, z_2, \dots\}$. This choice of observable functions is justified by the fact that polynomialization is an exact transformation, from the original state space to a higher dimension space; therefore, the lifted representation serves as a weak canonical form of the original system, given its nonuniqueness.

IV. NUMERICAL RESULTS

KOT is gaining momentum in the power system community [26]. A power system is chosen as a test system in this work because it has multiple attractors, and its model contains sine and cosine functions. Let us consider

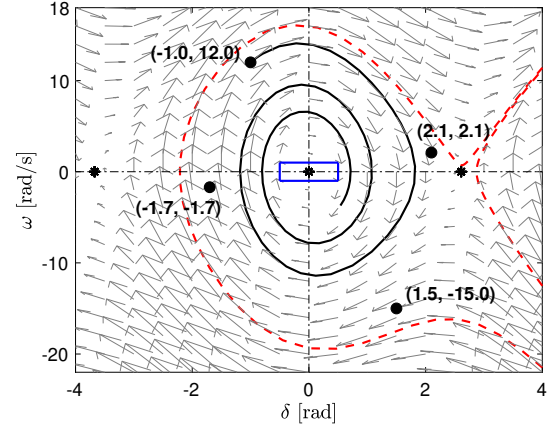


Fig. 1. Phase portrait of the dynamical system in (19)–(20). The symbol * denotes fixed points, and • denotes the initial states, (δ_0, ω_0) , in cases 1 to 4 in Fig. 3. The rectangle centered at the origin indicates the region where trajectories were sampled to compute EDMD. The dotted line --- delineates the attractor.

$$\dot{\delta} = \omega, \quad (19)$$

$$\dot{\omega} = \frac{1}{M} \left(k_1 + k_2 \cos \delta + k_3 \sin \delta - \frac{D}{\omega_s} \omega \right). \quad (20)$$

Details of the power system model (19)–(20) are provided in Appendix A, and its phase portrait is shown in Fig. 1. Trajectories with starting point (δ_0, ω_0) in the lattice $\delta = (-0.50 : 0.25 : 0.50)$, $\omega = (-1.00 : 0.25 : 1.00)$, are sampled at each $\Delta t = 0.005$ second. This sampling rate is consistent with the available technology for power system measurement devices, namely phasor measurement units. The lattice is indicated in Fig. 1 by the blue rectangle centered at the origin, and it contains 45 starting points, thereby leading to 45 sampled trajectories. Note that all the trajectories in the lattice are in a linear region of the state space. We record the initial 0.8 second of each trajectory, thereby leading to 160 samples per trajectory. These trajectories are used to compute EDMD.

Now, define $z_1 := \delta$, $z_2 := \omega$, $z_3 := \sin \delta$ and $z_4 := \cos \delta$. By applying the procedure outlined in Section III, we have

$$\dot{z}_1 = z_2, \quad (21)$$

$$\dot{z}_2 = \frac{1}{M} \left(k_1 + k_2 z_4 + k_3 z_3 - \frac{D}{\omega_s} z_2 \right), \quad (22)$$

$$\dot{z}_3 = \mathcal{L}_{\mathbf{f}} \sin \delta = \frac{\partial \sin \delta}{\partial \delta} \dot{\delta} + \frac{\partial \sin \delta}{\partial \omega} \dot{\omega} = z_2 z_4, \quad (23)$$

$$\dot{z}_4 = \mathcal{L}_{\mathbf{f}} \cos \delta = \frac{\partial \cos \delta}{\partial \delta} \dot{\delta} + \frac{\partial \cos \delta}{\partial \omega} \dot{\omega} = -z_2 z_3, \quad (24)$$

and (21)–(24) contain only monomials in z . The lifted dynamical system in z suggests the use of the following observable functions, $[z_1 \ z_2 \ z_3 \ z_4 \ z_2 z_3 \ z_2 z_4]^T$, which yields to:

$$\mathbf{g} = [\delta \ \omega \ \sin \delta \ \cos \delta \ \omega \sin \delta \ \omega \cos \delta]^T. \quad (25)$$

We compute EDMD using the observable functions given by (25), which we refer to as EDMD-Lie. Additionally, for comparison, we compute EDMD with other sets of observable functions that have been widely used in the literature. In what follows, EDMD-p \underline{N} denotes the case where all monomials of the state variables up to degree \underline{N} are used. For example, in the case of EDMD-p3:

$$\mathbf{g} = [\delta \ \omega \ \delta \omega \ \delta^2 \ \omega^2 \ \delta^2 \omega \ \delta \omega^2 \ \delta^3 \ \omega^3]^T. \quad (26)$$

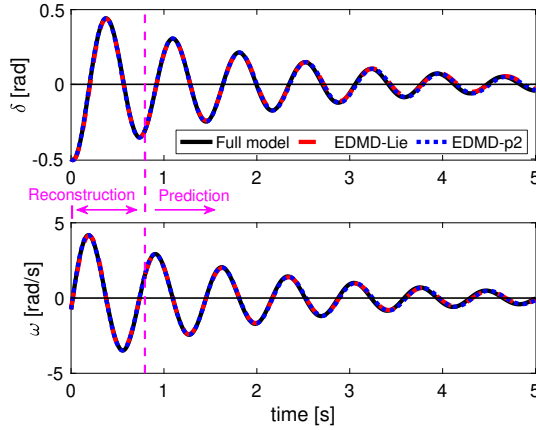


Fig. 2. Example of a trajectory starting at $(\delta_0, \omega_0) = (-0.50, -0.75)$, i.e., within the sampled region surrounding the fixed point $(0, 0)$ where trajectories were sampled to compute EDMD. The system mode is mildly damped, $D = \frac{10}{\omega_s}$, $\lambda_{\text{true}} = -0.5000 \pm j8.8503$, $f_{\text{true}} = 1.4086\text{Hz}$, and $\xi_{\text{true}} = 5.6406\%$.

We consider using all monomials of the state variables up to degree 2, 3, and 4, respectively denoted by EDMD-p2, EDMD-p3, and EDMD-p4. Further, the use of radial basis functions is also common in the literature. EDMD-rbfN denotes the case where the state variables, (δ, ω) , plus $N-2$ thin-plate spline radial basis functions with center at \mathbf{x}_c :

$$g(\mathbf{x}) = \|\mathbf{x} - \mathbf{x}_c\|^2 \log(\|\mathbf{x} - \mathbf{x}_c\|), \quad (27)$$

are used [15].

We consider two cases with radial basis functions. The first case, EDMD-rbf6, is designed to have the same size of the Lie lifted system. This will allow us to make a fair comparison between EDMD-Lie and the case where radial basis functions is used. The second case, EDMD-rbf19, is designed to exploit the maximum possible number of radial basis functions before the Koopman Kalman filter in Section IV-B becomes unobservable.

By linearizing (19)–(20) around the fixed point, $(0, 0)$, and by computing the eigenvalues of the obtained Jacobian matrix, one finds a pair of complex-conjugate eigenvalues, $\lambda_{\text{true}} = -0.5000 \pm j8.8503$, associated with the linear mode of frequency $f_{\text{true}} = 1.4086\text{ Hz}$ and damping ratio $\xi_{\text{true}} = 5.6406\%$. For comparison, the eigenvalues estimated through EDMD with different sets of observable functions are shown in Table III. The pairs of complex-conjugate eigenvalues associated with the linear mode, referred to as principal eigenvalues, are shaded in blue. A comparison between the dimension of the lifted model and the accuracy of the estimated principal eigenvalues is provided in Table IV. Note that the principal eigenvalues are well approximated in all cases; however, although estimating the linear mode with good numerical accuracy is important, this is only part of the information needed to represent the entire domain of attraction through the approximated Koopman tuples, $\{\lambda, \phi, v\}$.

A. Reconstruction and Prediction of Known Trajectories

To further assess the performance of EDMD with different sets of observables functions, we use the approximated Koopman tuples to reconstruct the trajectories given as inputs to EDMD. In Fig. 2, we show the results obtained with EDMD-Lie and EDMD-p2. We omit the results obtained with other sets of observable functions because they are quantitatively and qualitatively similar to EDMD-Lie. We observe that these trajectories do not pose any challenge to EDMD, independent of the choice of observable functions, because they are in a

TABLE III
EIGENVALUES ESTIMATED THROUGH EDMD WITH DIFFERENT SETS OF OBSERVABLE FUNCTIONS (PRINCIPAL EIGENVALUES ARE SHADED)

EDMD	Eigenvalues		
Lie	0.0529	$-0.5134 \pm j8.7623$	$-3.5394 \pm j17.7558$
	-5.4014		
p2	$-0.5011 \pm j8.7504$	$-0.9950 \pm j17.4716$	-1.0048
p3	$-0.4943 \pm j8.8511$	$-0.9961 \pm j17.4634$	-1.0095
	$-1.4837 \pm j26.1940$	$-1.4938 \pm j8.6778$	
p4	$-0.4949 \pm j8.8487$	$-0.9734 \pm j17.6953$	-1.0001
	$-1.4782 \pm j26.1682$	$-1.5271 \pm j8.6792$	$-1.9806 \pm j34.9201$
	-1.9844	$-2.0156 \pm j17.3382$	
rbf6	$-0.2218 \pm j1.3005$	$-0.5059 \pm j8.7427$	$-1.2829 \pm j14.2659$
rbf19	-0.0463	$-0.4976 \pm j8.7607$	$-1.2354 \pm j19.2201$
	$-2.4783 \pm j1.8160$	$-6.9312 \pm j11.6575$	$-7.7604 \pm j26.8570$
	$-9.1463 \pm j20.7501$	$-12.7618 \pm j51.9406$	$-16.5766 \pm j93.1681$
	$-31.6343 \pm j42.8542$		

TABLE IV
DIMENSION OF LIFTED MODEL VS. ESTIMATION ACCURACY OF THE PRINCIPAL EIGENVALUE, $\lambda_{\text{TRUE}} = -0.5000 \pm j8.8503$, $f_{\text{TRUE}} = 1.4086\text{Hz}$, AND $\xi_{\text{TRUE}} = 5.6406\%$

EDMD	Dimension of lifted model	Relative error in the principal eigenvalue		
		Real part [%]	Imaginary part [%]	ξ [%]
Lie	6	2.68	0.99	3.70
p2	5	0.22	1.13	1.36
p3	9	1.14	0.01	1.15
p4	14	1.02	0.02	1.00
rbf6	6	1.18	1.22	2.42
rbf19	19	0.48	1.01	0.54

linear region of the state space. In this case, however, it is difficult to assess whether EDMD is performing well or simply overfitting the input data.

B. Prediction of Strongly Nonlinear Trajectories by Applying the Koopman Kalman Filter

In theory, the Koopman operator is valid in the entire domain of attraction [27]; hence, the approximation of the Koopman operator via EDMD should provide the means to predict, with good numerical accuracy, any trajectory in the same domain of attraction for which EDMD was computed. This is when the choice of observable functions plays a key role—for example, it will directly affect the transient stability analysis [28] of electric power grids.

We use the approximated Koopman tuples to predict trajectories that start far from the fixed point and are strongly nonlinear. Further, these trajectories are not used as inputs to EDMD in first place. This test will reveal how well the Koopman tuples approximated by EDMD are representative of the entire domain of attraction. Four trajectories are selected, with initial states (δ_0, ω_0) indicated by \bullet in Fig. 1.

The Koopman tuples estimated through EDMD are used to design a robust Koopman Kalman filter (KKF) [22], [29], with real and reactive power measured at the generator terminal. Figs. 3a–3d compare the trajectory obtained with the KKF design with EDMD-Lie versus the full nonlinear model, (19)–(20), for each of the selected starting points. To avoid making the plot too crowded, Figs. 3a–3d do not show the trajectories obtained with the KKF design using other sets of observable functions; instead, we calculate the absolute error in δ and ω for each case and present their statistics in Table V. Also, the absolute error in δ is shown in Figs. 3e–3h.

Table V and Fig. 3 show that EDMD-Lie has overall better performance, indicating that the proposed analytical approach to ascertain observable functions captures the system dynamics well enough to predict unforeseen scenarios. In this illustration, the availability of the system model enabled us to make an informed decision on the selection of observable

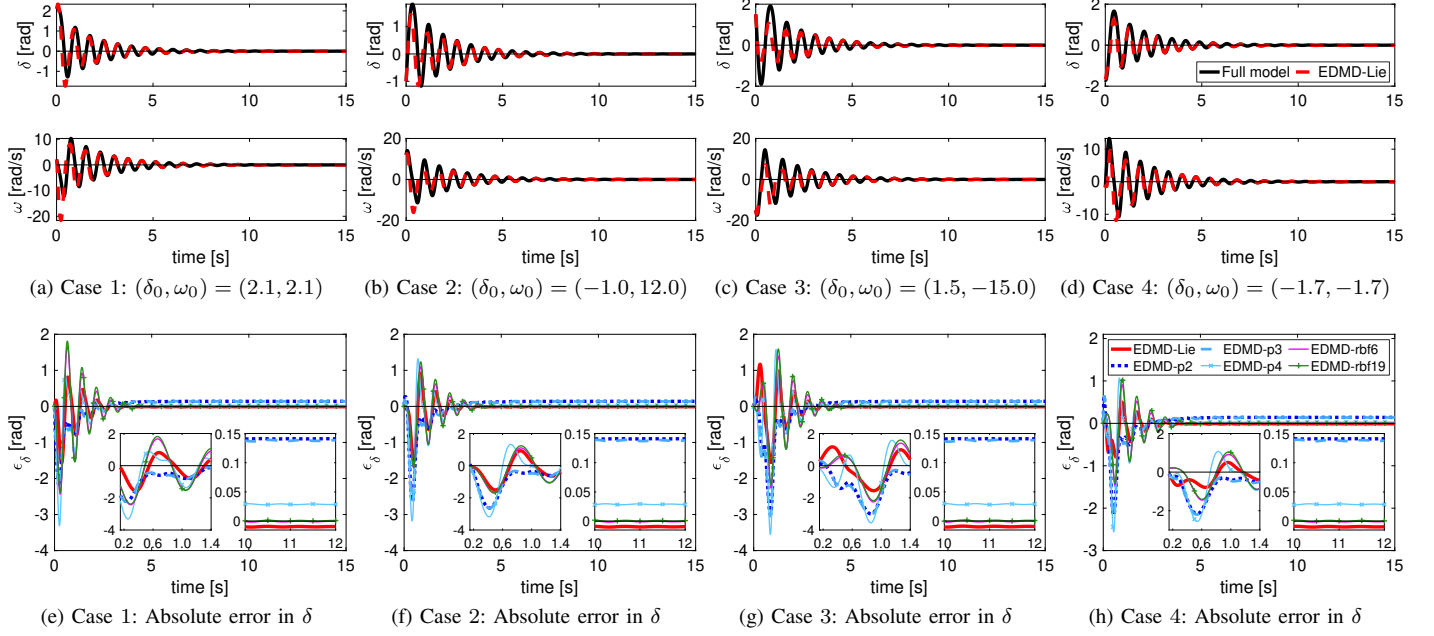


Fig. 3. Example of trajectories starting near the stability boundary.

TABLE V
STATISTICS OF THE ERRORS IN δ AND ω ASSOCIATED WITH CASES 1 TO 4 SHOWN IN FIG. 3 (THE LEAST ERROR IS SHADED)

Case	Statistics	EDMD					
		Lie	p2	p3	p4	rbf6	rbf19
1	$\max \epsilon_\delta$	1.5735	2.2180	2.2462	3.3128	2.4319	2.3863
	$\max \epsilon_\omega$	16.4016	18.0962	17.4020	28.5348	18.5667	18.7209
	$\sum \epsilon_\delta / 1e2$	2.3038	5.8993	5.9092	3.8766	4.1549	4.4859
	$\sum \epsilon_\omega / 1e3$	2.1847	6.4145	5.4323	4.2189	3.4940	3.8058
2	$\max \epsilon_\delta$	1.5096	2.6313	2.6418	3.1758	1.7058	1.6560
	$\max \epsilon_\omega$	14.6195	23.8467	21.9599	32.1051	12.8223	12.9307
	$\sum \epsilon_\delta / 1e2$	2.2946	5.9485	5.9178	3.8145	2.9216	3.1676
	$\sum \epsilon_\omega / 1e3$	2.1780	6.4989	5.4375	4.0880	2.3849	2.6352
3	$\max \epsilon_\delta$	1.5572	3.0010	3.0463	3.5522	2.2549	2.1697
	$\max \epsilon_\omega$	12.7739	29.5142	26.7154	36.9509	16.5962	16.7258
	$\sum \epsilon_\delta / 1e2$	3.0947	6.9762	7.1406	4.7190	3.8288	4.1487
	$\sum \epsilon_\omega / 1e3$	2.6237	8.2182	6.9028	5.8950	3.1748	3.4745
4	$\max \epsilon_\delta$	0.7924	2.1651	2.2015	2.5581	1.4498	1.4095
	$\max \epsilon_\omega$	9.2953	20.7167	19.1267	26.8149	10.8538	11.0328
	$\sum \epsilon_\delta / 1e2$	1.6953	5.6404	5.6739	3.2293	2.4925	2.7355
	$\sum \epsilon_\omega / 1e3$	1.5236	6.0980	5.1307	3.8430	2.0893	2.3331

functions; however, the procedure suggested here based on Lie derivatives can be applied even if the system model is not known a priori. For example, a system identification method based on KOT, e.g., the sparse identification of nonlinear dynamics [12], can be used to identify the elementary functions, $h(x)$. Then, in a second step, the system with elementary functions can be lifted to improve the performance of EDMD.

V. CONCLUSIONS AND FUTURE WORK

We provide an analytical method to select the observable functions to perform extended dynamic mode decomposition of nonlinear dynamics. This method is particularly attractive for dynamical systems where elementary nonlinear functions are beyond polynomial nonlinearities. The method can be applied to a broad class of nonlinear dynamical systems encountered in many engineering fields.

In future research, we will investigate the application of this method to power system models of increased complexity

and size, including wind turbine models and their data-driven control.

APPENDIX A SINGLE-MACHINE INFINITE BUS SYSTEM

Consider a synchronous generator represented by model 0.0 [30], also referred to as the classical model:

$$\dot{\delta} = \omega - \omega_s, \quad (28)$$

$$M\dot{\omega} + \frac{D}{\omega_s}(\omega - \omega_s) = P_m - P_e, \quad (29)$$

connected to an infinite bus, as shown in Fig. 4. In (28)–(29), δ is the electrical angle related to the rotor mechanical angle, ω is the angular velocity of the revolving magnetic field, $\omega_s = 2\pi f$ is the synchronous angular velocity of the revolving magnetic field, f is the system frequency, $M = 2H/\omega_s$ is the inertia constant, D is the damping constant, P_m is the mechanical power, and P_e is the electrical power.

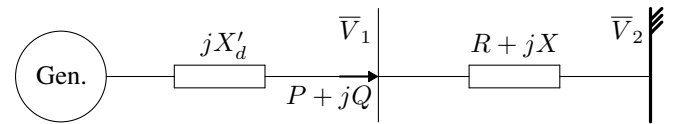


Fig. 4. One-line diagram of the single-machine infinite bus system. \bar{V}_1 , \bar{V}_2 are complex-valued voltage phasors in nodes 1 and 2, respectively. P (Q) is the real (reactive) power injected into node 1. R , X , and X'_d are parameters.

TABLE VI
SYSTEM DATA¹

R	X	V_1	V_2	P	X'_d	D	H	f
0.05	0.30	1.05	1.00	0.80	0.20	10	5	60

Fixed point:

Let $\bar{S} = P + jQ$ and $\bar{Y} = Ye^{j\gamma} = G + jB = \frac{1}{R + jX}$. Then:

¹Adapted from Example 2.3 in [31]. All values are given in per unit, except H , which is given in MJ/MVA, and f , which is given in Hz.

$$\begin{aligned}
\bar{S} &= \bar{V}_1 \bar{I}^* = V_1 e^{j\theta_1} (V_1 e^{-j\theta_1} - V_2 e^{j0}) Y e^{-j\gamma} \\
&= V_1^2 Y e^{-j\gamma} - V_1 V_2 Y e^{j(\theta_1 - \gamma)} \\
&= V_1^2 Y (\cos \gamma - j \sin \gamma) \\
&\quad - V_1 V_2 Y [\cos(\theta_1 - \gamma) + j \sin(\theta_1 - \gamma)], \quad (30)
\end{aligned}$$

\bar{I}^* is the complex-conjugate of the current phasor injected into node 1. Then:

$$\begin{aligned}
P &= \text{Re} \{ \bar{S} \} = V_1^2 Y \cos \gamma - V_1 V_2 Y \cos(\theta_1 - \gamma) \\
&= V_1^2 Y \cos \gamma - V_1 V_2 Y \cos \gamma \cos \theta_1 - V_1 V_2 Y \sin \gamma \sin \theta_1 \\
&= V_1^2 G - V_1 V_2 G \cos \theta_1 - V_1 V_2 B \sin \theta_1. \quad (31)
\end{aligned}$$

By substituting values into (31) and solving, $\theta_1 = 0.2243$. It follows that:

$$\begin{aligned}
\bar{I} &= (\bar{V}_1 - \bar{V}_2) \bar{Y} = 0.7718 e^{j0.0640}. \\
\bar{E} &= E e^{j\delta} = \bar{V}_1 + j X_d' \bar{I} = 1.0854 e^{j0.3651}.
\end{aligned}$$

$$\text{Let } \bar{S}_e = P_e + jQ_e \text{ and } \bar{Y}_{eq} = G_{eq} + jB_{eq} = \frac{1}{R + j(X + X_d')}.$$

Following (30)–(31), we obtain $P_e = E^2 G_{eq} - EV_2 G_{eq} \cos \delta - EV_2 B_{eq} \sin \delta$. Then:

$$\dot{\delta} = \omega - \omega_s, \quad (32)$$

$$M\dot{\omega} + \frac{D}{\omega_s} (\omega - \omega_s) = k_1 + c_2 \cos \delta + c_3 \sin \delta, \quad (33)$$

where $k_1 = P_m - E^2 G_{eq}$, $c_2 = EV_2 G_{eq}$, $c_3 = EV_2 B_{eq}$, and the fixed point $(\delta_0, \omega_0) = (0.3651, 2\pi f)$.

Shift fixed point to the origin:

Let $\delta = x_1 + \delta_0$ and $\omega = x_2 + \omega_0$. Then:

$$\dot{x}_1 = x_2 + \omega_0 - \omega_s = x_2.$$

$$\begin{aligned}
M\dot{x}_2 + \frac{D}{\omega_s} (x_2 + \omega_0 - \omega_s) &= M\dot{x}_2 + \frac{D}{\omega_s} x_2 \\
&= k_1 + c_2 \cos(x_1 + \delta_0) + c_3 \sin(x_1 + \delta_0) \\
&= k_1 + c_2 \cos x_1 \cos \delta_0 - c_2 \sin x_1 \sin \delta_0 \\
&\quad + c_3 \sin x_1 \cos \delta_0 + c_3 \sin \delta_0 \cos x_1.
\end{aligned}$$

Finally:

$$\dot{x}_1 = x_2, \quad (34)$$

$$M\dot{x}_2 + \frac{D}{\omega_s} x_2 = k_1 + k_2 \cos x_1 + k_3 \sin x_1, \quad (35)$$

where $k_2 = c_2 \cos \delta_0 + c_3 \sin \delta_0$ and $k_3 = c_3 \cos \delta_0 - c_2 \sin \delta_0$, and the fixed point $(x_{10}, x_{20}) = (0, 0)$. By substituting numerical values, $k_1 = 0.5667$, $k_2 = -0.5667$, and $k_3 = -2.0843$.

ACKNOWLEDGMENTS

M. Netto is supported by the Director's Postdoctoral Fellowship under the Laboratory Directed Research and Development program at NREL. Y. Susuki is supported in part by JST, PRESTO Grant No. JP-MJPR1926. V. Krishnan is supported by the U.S. Department of Energy Office of Electricity (DE-OE0000876).

REFERENCES

- [1] M. Budišić, R. Mohr, and I. Mezić, "Applied Koopmanism," *Chaos*, vol. 22, no. 4, p. 047510, 2012.
- [2] A. Mauroy, I. Mezić, and Y. Susuki (Editors), *The Koopman Operator in Systems and Control: Concepts, Methodologies, and Applications*. Springer Nature, 2020.
- [3] J. N. Kutz, S. L. Brunton, B. W. Brunton, and J. L. Proctor, *Dynamic Mode Decomposition: Data-Driven Modeling of Complex Systems*. SIAM, 2016.
- [4] A. Mauroy and J. Goncalves, "Koopman-Based Lifting Techniques for Nonlinear Systems Identification," *IEEE Transactions on Automatic Control*, vol. 65, no. 6, pp. 2550–2565, 2020.
- [5] A. Surana and A. Banaszuk, "Linear observer synthesis for nonlinear systems using Koopman Operator framework," *IFAC-PapersOnLine*, vol. 49, no. 18, pp. 716 – 723, 2016, 10th IFAC Symposium on Nonlinear Control Systems NOLCOS 2016.
- [6] A. Mauroy and I. Mezić, "Global Stability Analysis Using the Eigenfunctions of the Koopman Operator," *IEEE Transactions on Automatic Control*, vol. 61, no. 11, pp. 3356–3369, 2016.
- [7] M. Korda and I. Mezić, "Optimal construction of Koopman eigenfunctions for prediction and control," *IEEE Transactions on Automatic Control*, pp. 1–1, 2020.
- [8] M. O. Williams, I. G. Kevrekidis, and C. W. Rowley, "A Data-Driven Approximation of the Koopman Operator: Extending Dynamic Mode Decomposition," *Journal of Nonlinear Science*, vol. 25, no. 6, pp. 1307–1346, 2015.
- [9] M. Korda and I. Mezić, "On Convergence of Extended Dynamic Mode Decomposition to the Koopman Operator," *Journal of Nonlinear Science*, vol. 28, no. 2, pp. 687–710, 2018.
- [10] S. E. Otto and C. W. Rowley, "Linearly Recurrent Autoencoder Networks for Learning Dynamics," *SIAM Journal on Applied Dynamical Systems*, vol. 18, no. 1, pp. 558–593, 2019.
- [11] S. L. Brunton, B. W. Brunton, J. L. Proctor, and J. N. Kutz, "Koopman Invariant Subspaces and Finite Linear Representations of Nonlinear Dynamical Systems for Control," *PLOS ONE*, vol. 11, no. 2, pp. 1–19, 2016.
- [12] S. L. Brunton, J. L. Proctor, and J. N. Kutz, "Discovering governing equations from data by sparse identification of nonlinear dynamical systems," *Proceedings of the National Academy of Sciences*, vol. 113, no. 15, pp. 3932–3937, 2016.
- [13] Q. Li, F. Dietrich, E. M. Bollt, and I. G. Kevrekidis, "Extended dynamic mode decomposition with dictionary learning: A data-driven adaptive spectral decomposition of the Koopman operator," *Chaos*, vol. 27, no. 10, p. 103111, 2017.
- [14] B. Lusch, J. N. Kutz, and S. L. Brunton, "Deep learning for universal linear embeddings of nonlinear dynamics," *Nature Communications*, vol. 9, no. 1, p. 4950, 2018.
- [15] M. Korda and I. Mezić, "Linear predictors for nonlinear dynamical systems: Koopman operator meets model predictive control," *Automatica*, vol. 93, pp. 149 – 160, 2018.
- [16] K. Kowalski and W.-H. Steeb, *Nonlinear Dynamical Systems and Carleman Linearization*. World Scientific, 1991.
- [17] C. Gu, "QLMOR: A Projection-Based Nonlinear Model Order Reduction Approach Using Quadratic-Linear Representation of Nonlinear Systems," *IEEE Transactions on Computer-Aided Design of Integrated Circuits and Systems*, vol. 30, no. 9, pp. 1307–1320, 2011.
- [18] B. O. Koopman, "Hamiltonian Systems and Transformation in Hilbert Space," *Proceedings of the National Academy of Sciences*, vol. 17, no. 5, pp. 315–318, 1931.
- [19] C. W. Rowley, I. Mezić, S. Bagheri, P. Schlatter, and D. S. Henningson, "Spectral analysis of nonlinear flows," *Journal of Fluid Mechanics*, vol. 641, p. 115127, 2009.
- [20] D. Sigg, "Modeling ion channels: Past, present, and future," *Journal of General Physiology*, vol. 144, no. 1, pp. 7–26, 06 2014.
- [21] T. Grasser, T.-W. Tang, H. Kosina, and S. Selberherr, "A review of hydrodynamic and energy-transport models for semiconductor device simulation," *Proceedings of the IEEE*, vol. 91, no. 2, pp. 251–274, 2003.
- [22] M. Netto and L. Mili, "A Robust Data-Driven Koopman Kalman Filter for Power Systems Dynamic State Estimation," *IEEE Transactions on Power Systems*, vol. 33, no. 6, pp. 7228–7237, 2018.
- [23] M. Netto, Y. Susuki, and L. Mili, "Data-Driven Participation Factors for Nonlinear Systems Based on Koopman Mode Decomposition," *IEEE Control Systems Letters*, vol. 3, no. 1, pp. 198–203, 2019.
- [24] C. A. Johnson and E. Yeung, "A Class of Logistic Functions for Approximating State-Inclusive Koopman Operators," in *2018 Annual American Control Conference (ACC)*, 2018, pp. 4803–4810.
- [25] E. Qian, B. Kramer, B. Peherstorfer, and K. Willcox, "Lift & Learn: Physics-informed machine learning for large-scale nonlinear dynamical systems," *Physica D: Nonlinear Phenomena*, vol. 406, p. 132401, 2020.
- [26] Y. Susuki, I. Mezić, F. Raak, and T. Hikiyara, "Applied Koopman operator theory for power systems technology," *Nonlinear Theory and Its Applications, IEICE*, vol. 7, no. 4, pp. 430–459, 2016.
- [27] Y. Lan and I. Mezić, "Linearization in the large of nonlinear systems and Koopman operator spectrum," *Physica D: Nonlinear Phenomena*, vol. 242, no. 1, pp. 42 – 53, 2013.
- [28] P. Kundur, J. Paserba, V. Ajjarapu, G. Andersson, A. Bose, C. Canizares, N. Hatziairgiyriou, D. Hill, A. Stankovic, C. Taylor, T. Van Cutsem, and V. Vittal, "Definition and classification of power system stability IEEE/CIGRE joint task force on stability terms and definitions," *IEEE Transactions on Power Systems*, vol. 19, no. 3, pp. 1387–1401, 2004.
- [29] M. Netto and L. Mili, "Robust Koopman Operator-based Kalman Filter for Power Systems Dynamic State Estimation," in *2018 IEEE Power and Energy Society General Meeting (PESGM)*, 2018, pp. 1–5.
- [30] P. L. Dandeno, "Current Usage & Suggested Practices in Power System Stability Simulations for Synchronous Machines," *IEEE Transactions on Energy Conversion*, vol. EC-1, no. 1, pp. 77–93, 1986.
- [31] P. M. Anderson and A. A. Fouad, *Power System Control and Stability*, 2nd ed. Wiley, 2002.